13th International Symposium on Turbulence and Shear Flow Phenomena (TSFP13)
Montreal, Canada, June 25–28, 2024

LOW-FREQUENCY SPANWISE DYNAMICS OF A TURBULENT SEPARATION BUBBLE

Ben Steinfurth
Institute of Aeronautics and Astronautics
Technische Universität Berlin
Marchstraße 12-14, 10587 Berlin
ben.steinfurth@tu-berlin.de

Carolina Cura
Institute of Aeronautics and Astronautics
Technische Universität Berlin
Marchstraße 12-14, 10587 Berlin
c.cura@tu-berlin.de

Lukas Fuchs
Institute of Fluid Dynamics and Technical Acoustics
Technische Universität Berlin
Müller-Breslau-Straße 8, 10623 Berlin
l.fuchs@tu-berlin.de

Jakob G. R. von Saldern
Institute of Fluid Dynamics and Technical Acoustics
Technische Universität Berlin
Müller-Breslau-Straße 8, 10623 Berlin
j.vonsaldern@tu-berlin.de

Kilian Oberleithner
Institute of Fluid Dynamics and Technical Acoustics
Technische Universität Berlin
Müller-Breslau-Straße 8, 10623 Berlin
oberleithner@tu-berlin.de

Julien Weiss
Institute of Aeronautics and Astronautics
Technische Universität Berlin
Marchstraße 12-14, 10587 Berlin
julien.weiss@tu-berlin.de

ABSTRACT

In this study, the time-dependent behavior along the span of a turbulent separation bubble (TSB) occurring on an asymmetric diffuser is investigated ($U_\infty = 20\,\mathrm{m/s}$, $Re_\vartheta = 1000$). Spectral proper orthogonal decomposition (SPOD) is carried out based on unsteady measurements of the wall pressure and velocity in the region of flow separation and inside the TSB, respectively. The analysis suggests that the low-frequency unsteadiness, previously studied inside the symmetry plane, exhibits bi-modal behavior. According to the first mode, the wall pressure and streamwise velocity fluctuations are correlated throughout the TSB span. The second mode captures non-uniform fluctuations where the pressure/velocity decreases on one side of the test section and increases on the other (and vice versa). The two modes occur non-periodically and persist for varying periods of time that correspond to the low-frequency regime $\mathscr{O}(St) = 0.01$ associated with the breathing motion of TSBs (Mohammed-Taifour & Weiss, 2016).

1 INTRODUCTION

Confined near-wall regions of separated flow, or separation bubbles, are known to exhibit a variety of unsteady mechanisms that are manifested in pressure and velocity fluctuations at different time scales. For pressure-gradient-induced turbulent separation bubbles (TSBs), where a turbulent boundary layer separates because of an adverse pressure gradient and reattaches further downstream, particular attention has been drawn in recent years to a large-scale contraction and expansion of the recirculation region, dubbed breathing. This low-frequency unsteadiness was observed by Mohammed-Taifour & Weiss (2016) on a flat plate featuring a succession of adverse and favorable pressure gradients, by Richardson *et al.* (2023) on a similar configuration but featuring an adverse pressure gradient only, by Weiss *et al.* (2022) in a turbulent half-diffuser flow, and by Wang & Ghaemi (2022) in the TSB near the trailing edge of a two-dimensional wing. All these experiments, while performed in different wind tunnels, suggest a typical non-dimensional frequency $St = fL_\mathrm{b}/U_\infty \approx 0.01$, where L_b is the characteristic separation length and U_∞ the reference velocity in the wind tunnel.

Most experiments mentioned above captured the signature of the breathing motion using a variety of measurement techniques focused on the centerline of the respective wind tunnels. Hence, the spanwise dimension of the low-frequency breathing could not be examined. In contrast, Le Floc'h *et al.* (2018) performed spanwise measurements in the same configuration as Mohammed-Taifour & Weiss (2016) and concluded that the low-frequency breathing is strongly coherent in the spanwise direction, indicating a quasi-2D phenomenon. This conclusion was obtained by considering two-point cross-correlations of the unsteady wall-pressure only.

In the present contribution, we extend the work of Le Floc'h *et al.* (2018) and investigate the spanwise character of low-frequency unsteadiness in a turbulent half-diffuser. The three-dimensional mean flow topology for this setup was recently addressed by Steinfurth & Weiss (2024). In the present study, we use multi-point fluctuating pressure measurements in a spanwise array and high-frequency particle image velocimetry (PIV) in a spanwise wall-normal plane. This allows the use of spectral proper orthogonal decomposition (SPOD) to discover new insights into the spanwise dynamics of the flow.

2 METHODS

After introducing the flow geometry, including the low-frequency unsteadiness observed in the symmetry plane, we explain the experimental procedure and the employed data analysis techniques in the following.

2.1 Set-up: Low-frequency unsteadiness in the symmetry plane

The flow under consideration occurs in a two-dimensional test section with a span of $L_{sp} = 0.6$ m installed in a low-speed wind tunnel operated at $U_\infty = 20$ m/s. The Reynolds number, based on the momentum thickness of the incoming boundary layer $\vartheta \approx 0.79$ mm, is $Re_\vartheta \approx 1000$. The test section features a bottom surface segment of length $L = 0.34$ m that is inclined by $\varphi \approx 21°$, resulting in an axial diffuser extent of $L_D \approx 0.32$ m. In this one-sided diffuser, or backward-facing ramp, the kinetic energy decreases in the main flow direction and dynamic pressure is converted to static pressure. Due to the resulting adverse static pressure gradient, the near-wall momentum flux is reduced and, as a consequence, the boundary layer separates from the diffuser surface before reattaching further downstream on the test section floor. Early investigations of the flow dynamics in a similar configuration have been performed by Kaltenbach *et al.* (1999) using Large Eddy Simulations.

As first recognized by Mohammed-Taifour & Weiss (2016), the low-frequency dynamics of such turbulent separating and reattaching flows are governed by a large-scale coherent motion that can be readily captured by applying proper orthogonal decomposition (POD) to the streamwise velocity component. In the present study, a first mode representing more than 30% of the turbulent kinetic energy is found to represent a coherent region of correlated velocity fluctuations bounding the TSB (Figure 1). To illustrate the physical meaning of this mode, it is modulated with the minimum and maximum of the associated temporal coefficient (center and bottom contour plots in Figure 1), clearly indicating states of the contracted and expanded TSB. Specifically, compared to the mean TSB (dashed line) of length $L_b \approx 0.25$ m, the streamwise extent decreases for $\min(a_1)$ and increases for $\max(a_1)$.

To estimate the spectral content associated with the first POD mode, the normalized power spectral density (PSD) of the temporal coefficient a_1 is obtained using Welch's periodogram method (Figure 2).

A substantial proportion of the fluctuation energy is assigned to frequencies $St < 0.03$, rendering the breathing motion (i.e., the contraction/expansion of the TSB) a low-frequency phenomenon. As pointed out by Weiss *et al.* (2015), the low-frequency nature of the breathing phenomenon can also be revealed by pressure measurements. This is also true for the present set-up where the wall pressure signal measured on the diffuser center line just upstream of the location of mean separation exhibits substantial low-frequency content, agreeing well with the PSD of the first POD coefficient (Figure 2).

2.2 Acquisition of multi-point pressure and velocity signals

Despite the relative simplicity of the flow inside the symmetry plane addressed above, it is important to retain in mind that the diffuser flow is fully three-dimensional. Most prominently, the mean separation line (white line in Figure 3) is U-shaped as the boundary layer separates further upstream near the side walls, which is explained by the more substantial momentum deficit associated with the corner flow. Near the symmetry plane, the flow is accelerated to a greater extent at the diffuser entrance ($c_p < -0.2$, right-hand side in Figure 3), and mean separation only occurs approximately on the middle of the diffuser ramp. The curved separation line gives rise to a surface flow topology characterized by large-scale vortical secondary flow patterns of opposite sign on the top part of the diffuser ramp.

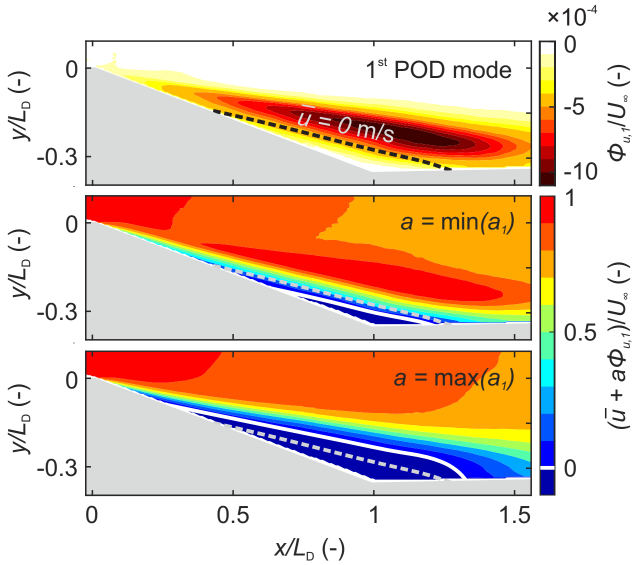

Figure 1. Classical POD analysis of streamwise velocity component in diffuser symmetry plane; top: first spatial POD mode, center and bottom: minimum/maximum representation of TSB as captured by first POD mode, dashed and solid lines highlight the $\bar{u}/U_\infty = 0$ iso-line of the mean and reconstructed velocity fields, respectively.

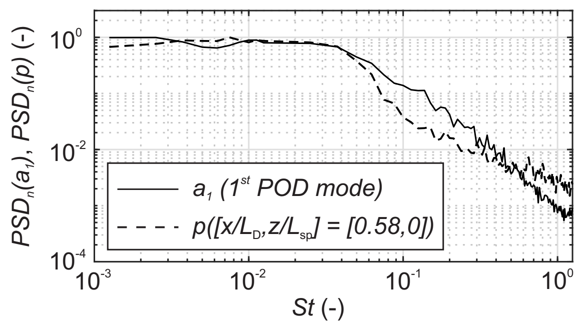

Figure 2. Frequency spectra for temporal coefficient related to first POD mode shown in Figure 1 and for wall pressure signal measured at location specified in legend; PSDs normalized by respective maxima.

In the present study, two types of measurements were conducted: the wall pressure was obtained quasi-simultaneously via seven pressure taps at $x/L_D = 0.58$, and the velocity field was measured inside a (zy)-cross-section at $x/L_D = 1.02$.

For the pressure measurements, piezo-resistive transducers with a temperature-compensated, amplified output in the range $p = [-249.1, 249.1]$ Pa at a sensitivity of $S \approx 8.03$ mV/Pa were employed. They were connected to pressure taps ($d = 0.5$ mm) via 20-mm long silicon tubes. Due to the combined volume of the tubes and the sensor cavity, a resonance frequency corresponding to $St \approx 7.5$ is observed, substantially exceeding the frequency regime relevant to the present study ($St < 1$). The spanwise spacing between the pressure taps was $\Delta z/L_{sp} \approx 0.14$; the locations were

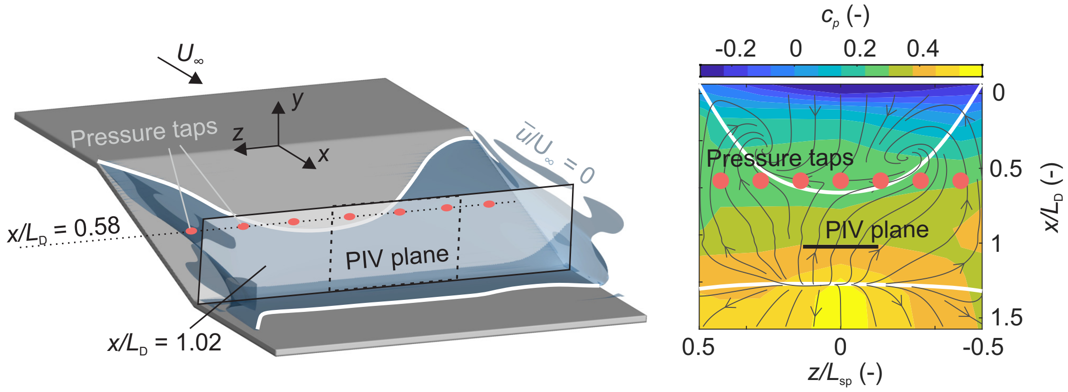

Figure 3. Three-dimensionality of one-sided diffuser flow; left: mean TSB indicated by blue iso-surface along with pressure and velocity measurement locations (red ellipses and dashed parallelogram, respectively), right: top view of wall pressure field overlayed with wall shear-stress lines.

$z = [0, \pm(0.14, 0.28, 0.42)]$ mm. Data were acquired for a duration of three minutes at a sampling frequency of 5 kHz, resulting in time series of 900,000 samples per location. Wind tunnel-inherent noise was reduced using an optimal Wiener filtering scheme (Naguib *et al.*, 1996). To this end, the wall pressure data obtained in the spanwise array were compared to a reference time series measured in the inflow at $x = -0.2$ m, and the common signal content was filtered.

In addition to pressure measurements, the velocity field was obtained in a cross-section at $x/L_D = 1.02$, covering the flow in the region $z/L_{sp} = [-0.14, 0.14]$ and $y/L_D = [-0.35, 0]$ in spanwise and wall-normal direction, respectively. DEHS seeding particles with a mean diamater of $d_{DEHS} = 1\,\mu$m were supplied to the flow downstream of the test section so that, after passing the closed-loop wind tunnel, a uniform tracer distribution was achieved inside the diffuser. The particles were illuminated by a *Litron LD30-527 PIV* laser where the laser beam was transformed to a light sheet with a maximum thickness of 3 mm. The scattered light was recorded using two *Phantom VEO 710* cameras (1280×800 px, $20\,\mu$m pixel pitch) that were installed downstream of the measurement plane, one on each side of the test section; the viewing angles were approximately 40 degrees (hence the angle enclosed by the viewing axes was 100 degrees). The focus planes were aligned with the light sheet by rotating each camera with respect to its lens (Scheimpflug principle). Snapshots were recorded at an acquisition rate of $f_s = 200$ Hz over a duration of 85 seconds, hence the time series spans 17,000 instantaneous velocity fields.

The snapshots were pre-processed by masking the light reflections on the diffuser surface and mean background subtraction before images were dewarped by applying a pin-hole calibration model with an average reprojection error of 0.5 pixels. In-plane velocity components w and v were computed using multi-grid cross-correlation with a final interrogation area size of $(24 \times 24)\,\text{px}^2$ or $(6.8 \times 6.8)\,\text{mm}^2$ at 12 px overlap (i.e., the vector pitch was 3.4 mm). Based on the two camera views, the out-of-plane component u was obtained. In doing so, a correction scheme was applied, reducing the disparity between the two camera views to within one pixel. Finally, a universal outlier detection (Westerweel & Scarano, 2005) was used to replace implausible vectors.

2.3 Implementation of spectral proper orthogonal decomposition and low-order modelling

SPOD has previously been proven as a suitable diagnostic to study separating and reattaching flows (Hoarau *et al.*, 2006; Ching & Eaton, 2020; Weiss *et al.*, 2022). Its advantage over the classical, or space-only, POD (Lumley, 1967) lies in its inherent capability to reveal the dynamics unfolding at specific frequencies.

In the present study, the input to the SPOD algorithm that is inspired by the works of Towne *et al.* (2018) and Schmidt & Colonius (2020) is either the fluctuating part of the pressure distribution $p'(\mathbf{x},t)$ or the streamwise velocity component $u'(\mathbf{x},t)$. The respective time signals are split into blocks spanning 10 seconds at an overlap of 5 seconds before being Fourier transformed using Welch's method (Bendat & Piersol, 2010). This results in data matrices $\hat{S}$ of size $N_b \times N_x \times N_f$ where $N_b = [35, 16]$ denotes the number of blocks, $N_x = [7, 1470]$ the number of measurement locations and $N_f = [25001, 1001]$ the number of frequency bins for the pressure and velocity analysis, respectively. Next, cross-spectral density (CSD) matrices $M = (\hat{S}_f^* \hat{S}_f)/(N_b - 1)$ are constructed by left-multiplying the data matrix (one frequency at a time) with its conjugate transpose. Analogous to the space-only POD, spatial modes are now obtained by an eigendecomposition and subsequent projection of the eigenvectors onto the unsteady (measurement) data. However, whereas this is carried out for one covariance matrix in the case of space-only POD, a modal decomposition of the CSD matrix can be performed for each frequency bin by means of SPOD.

The original data (p' and u') can be approximately recovered by inverting the procedure described above (i.e., by multiplying the expansion coefficients with the complex modes before applying inverse Fourier transformation). As we are interested in the low-frequency dynamics captured by individual modes in the present study, only the corresponding entries are taken into account when building low-order models of the pressure and velocity fluctuations. Specifically, only the leading and sub-leading modes are considered at frequencies up to $St = 0.0375$ ($f = 3$ Hz), spanning 301 frequency bins for pressure and 31 bins for the velocity analysis. The remaining frequency bins are zero-padded.

3 SPANWISE DYNAMICS

After providing an overview of the time-averaged pressure and velocity distributions, we will turn our attention to the

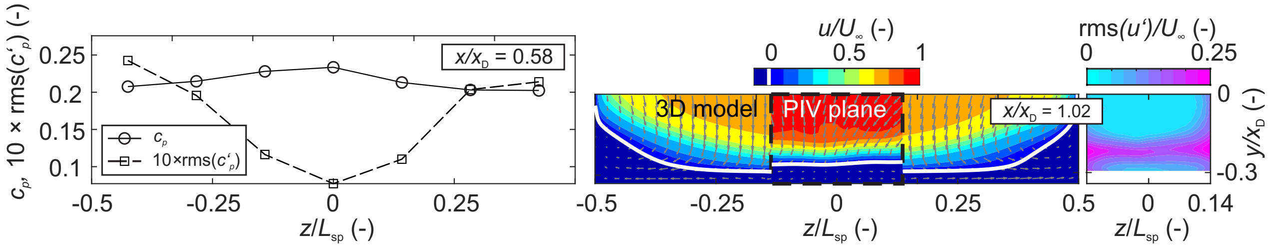

Figure 4. Left: Mean and fluctuating pressure distribution along the spanwise direction at $x/L_\mathrm{D} = 0.58$; right: mean and fluctuating streamwise velocity component inside a cross-section at $x/L_\mathrm{D} = 1.02$, the velocity field addressed in the present study lies in the range $z/L_\mathrm{sp} = [-0.14, 0.14]$ mm, a slice of a 3D model (Steinfurth & Weiss, 2024) is presented in the remainder of the cross-section

spanwise dynamics with particular focus on the low-frequency regime.

3.1 Mean and fluctuating parts of pressure and velocity distributions

The mean pressure distribution measured at $x/L_\mathrm{D} = 0.58$ (i.e., close to the location of mean flow separation in the symmetry plane) exhibits a global maximum on the center line while reduced pressure coefficients are found near the sidewalls (solid line in Figure 4). Fully consistent with the two-dimensional pressure distribution shown in Figure 3, the decreasing pressure recovery for larger $|z|$ is explained by the blocking effect of the recirculation zone that has a larger wall-normal extent near the sidewalls. At the same time, larger pressure fluctuations are observed in this region ($\mathrm{rms}(c_p')$, indicated by the dashed line, is twice as large as on the centerline), which may be explained by the dynamics of the corner flow. Similar effects were documented in the TSB of Le Floc'h *et al.* (2018).

The mean and fluctuating part of the velocity field inside the cross-section at $x/L_\mathrm{D} = 1.02$ (i.e., at the diffuser foot, in the middle of the TSB) are shown on the right-hand side of Figure 4. The color range reflects the streamwise/out-of-plane component while the mean in-plane components are indicated by arrows. The fluctuating part of the velocity component is consistent with the first POD mode shown in Fig. 1, indicating maximum fluctuations inside the shear layer that is bounding the TSB.

The mean flow inside the volumetric flow domain was recently assimilated using physics-informed neural networks based on experimental data (Steinfurth & Weiss, 2024). The velocity field exterior of the PIV plane is extracted from this model, indicating an increased extent of the TSB near the sidewalls accompanied by outward directed near-wall flow. Near the symmetry plane ($z/L_\mathrm{sp} = [-0.14, 0.14]$ mm), the measurement data drawn upon in the present study are presented. It is apparent that there is a mismatch between the two velocity distributions, which may be explained by a variability in the TSB dimensions owing to the strong sensitivity of a flow separating from a flat surface. Furthermore, a bias towards larger particle displacements may be caused by depth correlation errors introduced by the simple pinhole model used for the geometric camera calibration in the present study. Lastly, one should recall that the dimensions of interrogation areas (6.8 mm) are large compared to the velocity gradient inside the shear and boundary layers. As a result, the measurement accuracy may be affected by the large ratio between the variation of particle-image displacement and particle-image diameter (Keane & Adrian, 1990). Nonetheless, we proceed with the dynamical analysis as we do not expect the potential experimental shortcomings to affect the results from a qualitative perspective.

In the remainder of this article, focus is laid upon the time-dependent behavior of the pressure and velocity distributions.

First, time traces over the duration of 10 seconds are presented in Figure 5 along the spanwise direction inside the available measurement regions (i.e., $z/L_\mathrm{sp} = [-0.425, 0.425]$ for pressure and $z/L_\mathrm{sp} = [-0.14, 0.14]$ for velocity). In the case of the velocity component, the two-dimensional field is probed at a wall-normal distance of $\Delta y = 15$ mm. For reasons of clarity, only every 100th timestep is shown for the pressure signal and every fourth for the velocity time trace, yielding undersampled frequencies of 50 Hz for both cases.

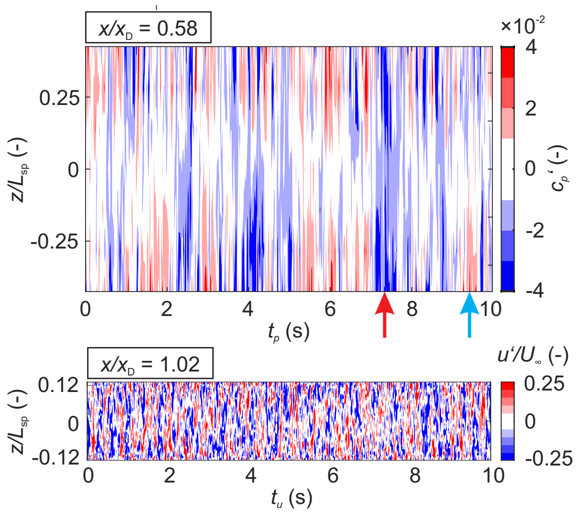

Figure 5. Top: pressure time trace ($x/L_\mathrm{D} = 0.58$), bottom: velocity time trace at a wall-normal distance of $\Delta y = 15$ mm ($x/L_\mathrm{D} = 1.02$).

As touched upon above, the largest pressure fluctuations are observed near the sidewalls, occasionally reaching values of $c_p' = \pm 0.04$. It is worth pointing out that the time scales associated with these fluctuations (for each sensor location individually) are on the order of one second, which corresponds to a Strouhal number of $St \approx 0.01$ and falls within the low-frequency regime associated with the breathing motion. For reference, the spectrum for the center location $z/L_\mathrm{sp} = 0$ is presented in Figure 2. Furthermore, there appears to be a two-fold systematic in terms of the fluctuations along the TSB/diffuser span. Either c_p' is correlated throughout z - in other words, the pressure increases/decreases at all measurement locations (e.g., $t_p \approx 7.5\,\mathrm{s}$, red arrow); or the fluctuations near both sidewalls are anti-correlated (e.g., $t_p \approx 9.5\,\mathrm{s}$, blue arrow).

The same is not immediately obvious in the case of the velocity time trace (bottom of Figure 5), which may be explained by the measurement field being restricted to the flow near the symmetry plane (where pressure fluctuations are the smallest) and the notion that instantaneous velocities are of a more localized nature compared to the pressure.

3.2 SPOD analysis

To investigate the spanwise characteristics of the unsteadiness in more detail, we compute the SPOD both of the pressure and velocity signals as described in the previous section. The SPOD eigenvalues are shown in Figure 6.

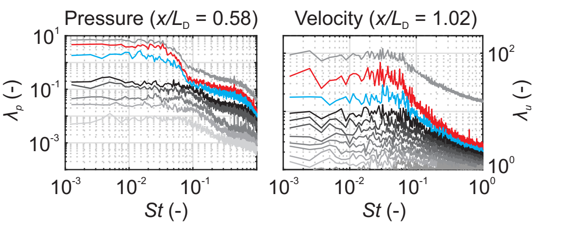

Figure 6. SPOD eigenvalue spectra; left: pressure, right: streamwise velocity component, red and blue lines highlight first and second modes, respectively; the upper gray line marks the sum of eigenvalues (for each frequency).

As for the pressure signal (left-hand side), the eigenvalues at low frequency ($St < 0.05$) reveal two strongly dominant modes. Specifically, in this frequency range, the following eigenvalues are at least an order of magnitude smaller. Similar low-rank behavior pertaining to the SPOD spectrum has previously been noted by Weiss *et al.* (2022) for unsteady wall shear-stress measurements conducted on the center line of the diffuser. However, as opposed to one dominant mode in that study, there is a secondary mode in the present investigation, whose physical meaning will be addressed shortly.

The real parts of the first two modes at a representative frequency of $St = 0.0125$ ($f = 1\,\mathrm{Hz}$) are shown in Figure 7. Both for the wall pressure and the velocity, the two modes clearly capture differing dynamics: Whereas the first mode is relatively constant across the span, the second changes sign. This indicates that the first mode describes a quasi-2D motion that is nearly homogeneous across the span, while the second mode portrays a low-frequency behavior that switches from left to right on the ramp. It is worth pointing out that these two modes can be identified by visual inspection in the pressure time trace (Figure 5).

To better understand the effect of these modes, we build low-order models of the pressure and velocity fluctuations. As explained in Sec. 2.3, we consider either the first or the second modes up to a Strouhal number of $St = 0.0375$ ($f = 3\,\mathrm{Hz}$), where the low-rank behavior is evident from Figure 6. Time traces of the modelled fluctuations are shown as time-space contour plots in Figure 8.

The presence of the two modes is evident in the pressure time trace: in several periods, c_p increases or decreases everywhere across the span. This is indicative of a quasi-2D behavior. In contrast, the second mode reveals other periods where the pressure increases on the left but decreases on the right

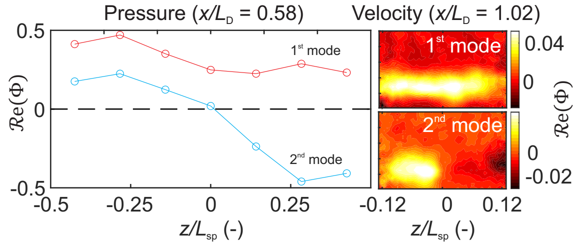

Figure 7. Real parts of first two SPOD modes for $St = 0.0125$; left: pressure, right: streamwise velocity component.

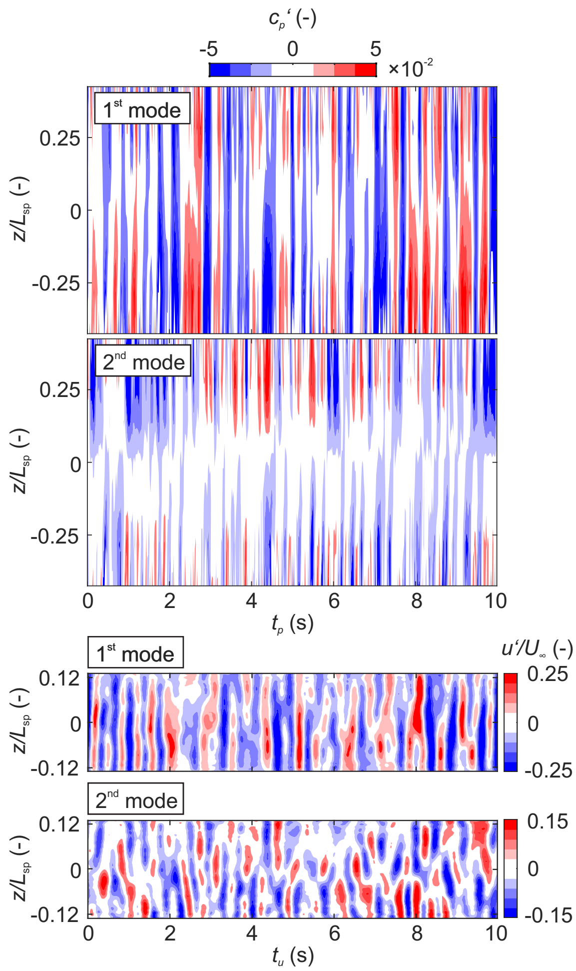

Figure 8. Low-order models of the same time traces as shown in Figure 5, $f < 3\mathrm{Hz}$.

(or vice versa), thus demonstrating a more complex behavior alternating from left to right.

While acknowledging that the velocity field measurements were limited to the range $z/L_{\mathrm{sp}} = [-0.14, 0.14]\,\mathrm{mm}$, an identical picture is revealed: whereas the first mode maps a quasi-2D motion of the TSB, spanwise inhomogeneities are expressed by the sub-leading mode.

4 CONCLUSIONS

In the present study, we investigated a TSB occuring in a one-sided diffuser. For this set-up, it has been found previously that the recirculation zone, when viewed in its symmetry plane, contracts and expands at time scales corresponding to $\mathcal{O}(St) = 0.01$ (Weiss *et al.*, 2022). Both the nature of this breathing motion and the associated Strouhal number are consistent with findings obtained for a different experimental set-up by Mohammed-Taifour & Weiss (2016).

The objective in the present effort was to shed some light on the three-dimensionality of this low-frequency unsteadiness. To this end, pressure and velocity measurements were conducted in a spanwise array and a cross-section of the flow, respectively. The SPOD analysis of the acquired time-dependent signals suggests that the breathing motion may be a quasi-2D phenomenon as the leading modes inside the relevant frequency range indicate uniform pressure and velocity fluctuations throughout the TSB span. This finding is consistent with two-point cross-correlations of the unsteady wall-pressure measured over the span by Le Floc'h *et al.* (2018). However, a secondary mode of similar energy is found in the present study, capturing anti-correlated fluctuations on both sides of the TSB. The latter are particularly prominent near the sidewalls where only the wall pressure (but not the velocity) could be measured in the present study. This may explain why distinct low-rank behavior is only found in the case of the pressure analysis.

Future efforts will be directed at validating whether low-rank behavior characterized by the two dominant modes is found for velocity fields extending to the sidewalls. Furthermore, the physical meaning of the two dominant spanwise modes will be explored, as it remains unclear if their dynamics is inherent to the separation bubble or an effect of the side walls. Finally, the SPOD results presented in this article will serve as a basis for comparison with future linear stability and resolvent analyses.

REFERENCES

Bendat, J. S. & Piersol, A. G. 2010 *Random data: Analysis and measurement procedures*. New York: Wiley.

Ching, D. S. & Eaton, J. K. 2020 Large-eddy simulation study of unsteady wake dynamics and geometric sensitivity on a skewed bump. *J. Fluid Mech.* **885**.

Hoarau, C., Borée, J., Laumonier, J. & Gervais, Y. 2006 Analysis of the wall pressure trace downstream of a separated region using extended proper orthogonal decomposition. *Phys. Fluids* **18** (5).

Kaltenbach, H-J, Fatica, M, Mittal, R, Lund, TS & Moin, P 1999 Study of flow in a planar asymmetric diffuser using large-eddy simulation. *Journal of Fluid Mechanics* **390**, 151–185.

Keane, R. D. & Adrian, R. J. 1990 Optimization of particle image velocimeters. Part I: Double pulsed systems. *Meas. Sci. Technol.* **1**, 1202–1205.

Le Floc'h, A., Mohammed-Taifour, A., Dufresne, L. & Weiss, J 2018 Spanwise aspects of unsteadiness in a pressure-induced turbulent separation bubble. In *AIAA 2018 Aviation*.

Lumley, J. L. 1967 The structure of inhomogeneous turbulent flows. *Atm. Turb. Radio Wave Propag.* pp. 166–178.

Mohammed-Taifour, A. & Weiss, J. 2016 Unsteadiness in a large turbulent separation bubble. *J. Fluid Mech.* **799**, 383–412.

Naguib, A. M., Gravante, S. P. & Wark, C. E. 1996 "extraction of turbulent wall- pressure time-series using an optimal filtering scheme. *Exp. Fluids* **22**, 14–22.

Richardson, R., Zhang, Y. & Cattafesta, L. N. 2023 Low frequency characteristics of a pressure-gradient induced turbulent separation bubble. In *AIAA SciTech 2023 Forum*.

Schmidt, O. T. & Colonius, T. 2020 Guide to spectral proper orthogonal decomposition. *AIAA J.* **58** (3), 1023–1033.

Steinfurth, B. & Weiss, J. 2024 Assimilating experimental data of a mean three-dimensional separated flow using physics-informed neural networks. *Phys. Fluids* **36** (1).

Towne, A., Schmidt, O. T. & Colonius, T. 2018 Spectral proper orthogonal decomposition and its relationship to dynamic mode decomposition and resolvent analysis. *J. Fluid Mech.* **847**, 821–867.

Wang, Sen & Ghaemi, Sina 2022 Unsteady motions in the turbulent separation bubble of a two-dimensional wing. *Journal of Fluid Mechanics* **948**, A3.

Weiss, J., Mohammed-Taiffour, A. & Schwab, Q. 2015 Unsteady behavior of a pressure-induced turbulent separation bubble. *AIAA J.* **53** (9), 2634–2645.

Weiss, J., Steinfurth, B., Chamard, L., Giani, A. & Combette, P. 2022 Spectral proper orthogonal decomposition of unsteady wall shear stress under a turbulent separation bubble. *AIAA J.* **60** (4), 2150–2159.

Westerweel, J. & Scarano, F. 2005 Universal outlier detection for PIV data. *Exp. Fluids* **39**, 1096–1100.